Journal of Zhejiang University-SCIENCE A (Applied Physics & Engineering)
ISSN 1673-565X (Print); ISSN 1862-1775 (Online)
www.jzus.zju.edu.cn; link.springer.com
E-mail: jzus_a@zju.edu.cn

Effects and mechanisms of surfactants on physical properties and microstructures of metakaolin-based geopolymer*

Dong-ming YAN[1], Sheng-qian RUAN[1], Shi-kun CHEN[†‡1],
Yi LIU[2], Ye TIAN[1], Hai-long WANG[1], Tian-nan YE[3]
[1]*School of Civil and Architectural Engineering, Zhejiang University, Hangzhou 310058, China*
[2]*School of Materials Science and Engineering, Zhejiang University, Hangzhou 310027, China*
[3]*Materials Research Center for Element Strategy, Tokyo Institute of Technology, 4259 Nagatsuta, Midori-ku, Yokohama 226-8503, Japan*
[†]E-mail: chen_sk@zju.edu.cn

Received Feb. 15, 2020; Revision accepted May 28, 2020; Crosschecked Dec. 24, 2020; Published online Jan. 25, 2021

Abstract: In this study, the effects of five different ionic and nonionic surfactants on the physical properties and microstructures of a metakaolin-based geopolymer (MKG) were investigated. It is the first comprehensive comparative study of the effects of sodium lauryl sulfonate (SLS), alkyl polyglycoside (APG), benzalkonium chloride (BAC), sucrose fatty acid esters (SE), and stearic acid (STA) on MKG. Viscosity, densities, apparent water absorption, and compressive strength were measured, and pore structures, micro-defects, and gels observed through scanning electron microscopy (SEM) and mercury intrusion porosimetry (MIP). In the MKG slurry, a high affinity of surfactants to liquid-air interfaces increased viscosity and promoted the generation of bubbles. Based on both the ionic types and molecular configurations of the surfactants, stronger adsorption of a surfactant on the surface of the metakaolin resulted in better dispersion of metakaolin particles and a denser microstructure of the MKG. The surfactants with weaker adsorption (SLS and APG) caused higher porosity, a larger pore size, and more micro-defects, while those with stronger adsorption (BAC, SE, and STA) led to relatively lower porosity and denser microstructures. Density, water absorption, and compressive strength were closely related to the total intrusion porosity of the MKG. The mechanisms underlying surfactant adsorption to the surface of metakaolin are proposed.

Key words: Metakaolin-based geopolymer (MKG); Surfactants; Physical properties; Microstructure; Adsorption; Microscopic mechanism
https://doi.org/10.1631/jzus.A2000059 **CLC number:** TU523

1 Introduction

Geopolymers are synthetic materials manufactured using aluminosilicate raw materials with a highly concentrated aqueous alkali hydroxide or silicate solution (Duxson et al., 2007a). In addition to the properties of high mechanical strength (Palomo et al., 1992; Duxson et al., 2005), strong bonding performance (Kriven et al., 2006), and fast and controllable setting (Lee and van Deventer, 2002), geopolymers have great durability, including strong chemical resistance (Palomo et al., 1992; Duxson et al., 2007b), high temperature resistance (Lyon et al., 1997; Kong et al., 2007, 2008), and antifreeze capacity (Slavik et al., 2008). These outstanding properties make them suitable for onshore and offshore engineering buildings exposed to harsh natural conditions. Because of the lower energy consumption and lower CO_2 emissions involved in their manufacture (Turner and Collins, 2013), geopolymers are also regarded as

---

‡ Corresponding author

* Project supported by the National Key R&D Program of China (No. 2018YFB0605700) and the National Natural Science Foundation of China (Nos. 51879230 and 51978608)

ORCID: Shi-kun CHEN, https://orcid.org/0000-0002-3160-4101 superior to ordinary Portland cement in terms of energy conservation and environmental protection.

Manipulating the microstructure of geopolymers is a feasible approach to regulating their mechanical properties (Duxson et al., 2005) and durability (Ismail et al., 2013b; Nasvi et al., 2014; Zhang and Wang, 2015). Extensive test data indicates that their microstructure is affected by their raw materials (Morsy et al., 2014; Duan et al., 2016; Tchakouté et al., 2018), mixture proportions (Rowles and O'connor, 2003; Duxson et al., 2005; Brylewska et al., 2018), and curing conditions (Rovnaník, 2010; Baščarević et al., 2013; El-Naggar and El-Dessouky, 2017). In addition, chemical additives used as modifiers have attracted attention, and have been used to synthesize geopolymers with high quality and good performance (Tchakouté et al., 2018).

Surfactants, as amphiphilic compound additives, are widely used in the dispersion of additives for geopolymers such as carbon nanotubes (Yang et al., 2014; Parveen et al., 2015; MacLeod et al., 2019), graphene oxide (Zhao et al., 2018; Wang and Deng, 2019), carbon microspheres (Saleh and Ali, 2018), fibers (Curosu et al., 2017; He et al., 2017), and mineral admixtures (Külaots et al., 2003; Naden, 2016). However, the surfactant will also affect the geopolymer through its adsorption onto the surface of raw materials, gels, and interphase boundaries (Mulligan et al., 2001; Zhang et al., 2001). Previous studies have revealed that surfactants can optimize the bubble generation, pore distribution and microstructure of geopolymers (Masi et al., 2014; Bai and Colombo, 2017; Samson and Cyr, 2018). Protein-type surfactants cause a reduction of open porosity and total porosity in metakaolin-based geopolymer (MKG) (Bai et al., 2018). The cationic surfactant cetylpyridinium chloride (CPC) promotes a mixed ordered-disordered hierarchical meso-structure of geopolymers, which exhibit a narrow pore size distribution and a large pore volume (Yuan et al., 2002). The nonionic surfactant Triton X-100 accelerates the generation of a homogeneous microstructure of geopolymers in open cells (Bai et al., 2018). For cement-based materials, the use of some surfactants can lead to smaller pore size, lower porosity (Ouyang et al., 2008), and higher strength (Sarda et al., 2003). These surfactants facilitate the better dispersion of cement particles, and promote the entanglement and densification of the microstructure (Wang and Zhang, 2014). Other surfactants tend to produce high levels of total porosity and interconnected cell structures (Cilla et al., 2014).

Nonetheless, the complex effects of surfactants on the microstructure and properties of geopolymers have not been comprehensively studied. Furthermore, the underlying mechanisms have not been discussed, especially in terms of surfactant molecules. Therefore, it is important to systematically explore the effects of surfactants on geopolymers.

In this work, five different ionic and nonionic surfactants including sodium lauryl sulfonate (SLS), alkyl polyglycoside (APG), benzalkonium chloride (BAC), sucrose fatty acid esters (SE), and stearic acid (STA) were studied. Their effects on the viscosity, density, apparent water absorption, compressive strength, and microstructure, including pore structures, micro-defects, and gels, of an MKG were explored. Furthermore, the underlying mechanisms of surfactant adsorption onto the metakaolin surface are proposed, and relevant recommendations are provided for the research and engineering applications of surfactants to geopolymers.

2 Materials and experimental methods

2.1 Materials

2.1.1 Metakaolin

The industrial Metamax metakaolin used to make geopolymer paste was bought from BASF SE (Germany). The chemical composition of the metakaolin, tested by an X-ray fluorescence (XRF) method using a Thermo Fisher Scientific ARL XRF analyzer (USA), is shown in Table 1. The morphology of metakaolin particles obtained through scanning electron microscopy (SEM) is shown in Fig. 1, and the distribution of particle size obtained using a Mastersizer 2000 laser particle size analyzer (UK) is shown in Fig. 2. The average particle diameter of the metakaolin powder was around 5.91 μm, and 90% of the particles were smaller than 13.59 μm.

2.1.2 Alkaline activator

An alkaline activator solution was obtained by mixing sodium silicate solution and sodium hydroxide solid at a mass ratio of 9.25:1. Sodium hydroxide solid was added to the sodium silicate solution, and the mixed solution was stirred until the solid was completely dissolved. Then the alkaline activator at ambient temperature and clearance was prepared for use. The alkaline activator modulus of the silicate (equivalent to the SiO_2/Na_2O molar ratio in the activator solution) was 1.62, and the water content was 39.37%.

Table 1 Composition of the metakaolin

Component	Mass content (%)	Component	Mass content (%)
Al_2O_3	42.45	K_2O	0.15
SiO_2	54.25	MgO	0.14
TiO_2	1.87	P_2O_5	0.09
Fe_2O_3	0.48	CaO	0.07
Na_2O	0.29	Other	0.21

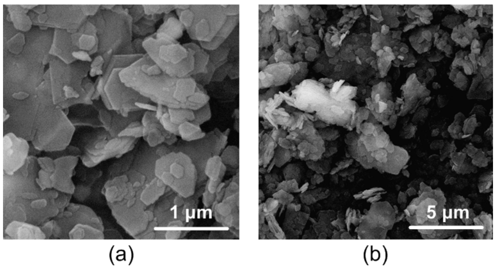

Fig. 1 Morphology of metakaolin particles obtained through SEM

(a) Magnification of 100000; (b) Magnification of 20000

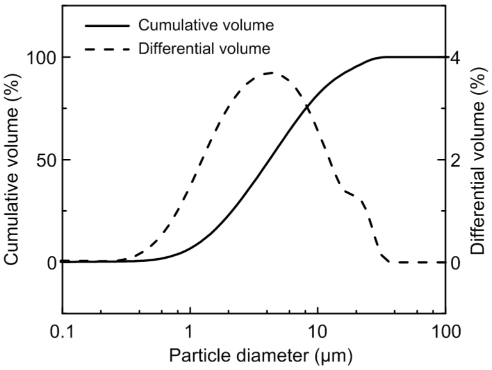

Fig. 2 Distribution of metakaolin particle size

The sodium silicate solution, produced by Hengli Chemical Co., Ltd., China had a molar ratio of SiO_2/Na_2O of about 3.28 (SiO_2=26.0% (in weight), Na_2O=8.2% (in weight)). The sodium hydroxide, produced by Sinopharm Chemical Reagent Co., Ltd., China was a flaked solid with analytical purity (AR) of ≥96%.

2.1.3 Surfactants

Five cationic, anionic, and nonionic surfactants were used in experiments. BAC is an important kind of quaternary ammonium salt cationic surfactant containing a hydrophobic benzene ring. Generally, STA reacts to form stearates with surface activity in strong alkaline solution, and is regarded as an anion surfactant for a geopolymer system. SLS is also an anion surfactant, but the hydrophilic head and the length of the stretched hydrocarbon chain are different from those of STA. APG is a nonionic surfactant with a relatively complex structure. The molecule contains a large hydrophilic head with four hydroxyl groups and two ether groups, and a hydrophobic hydrocarbon tail of 12 carbon atoms. SE is a nonionic surfactant that partially decomposes into stearates (the same as STA) and hydrophilic molecules in alkaline solution. So, it is considered to provide both nonionic and anionic surfactants in a geopolymer system.

Table 2 lists details of the five surfactants. pH values were measured at a concentration of additive/water equal to 1 g/100 mL at the room temperature of 24.5 °C and atmospheric pressure of 101.1 kPa. The effective structural formula, electric charge, and length of the stretched hydrocarbon chain of each surfactant are shown in Fig. 3.

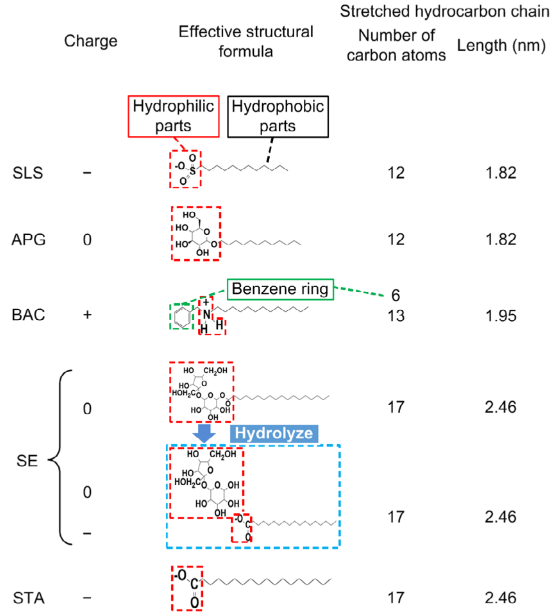

Fig. 3 Effective structural formula, electric charge, and length of stretched hydrocarbon chain of different surfactants

2.2 Paste mixes

According to their elemental composition, the mass ratio of the three raw materials (metakaolin: sodium silicate solution:sodium hydroxide solid) was determined as 5.79:9.25:1. Thus, the molar ratio of the three main elements (n_{Si}:n_{Al}:n_{Na}) in the geopolymer was 1.85:0.96:1. The calculation process was as follows:

$$n_{\mathrm{Si}}:n_{\mathrm{Al}}:n_{\mathrm{Na}}=\left[\frac{m_{\mathrm{MK}}a_1+m_{\mathrm{SS}}b_1}{M_1}\right]:\left[\frac{2m_{\mathrm{MK}}a_2}{M_2}\right]:\left[\frac{2(m_{\mathrm{MK}}a_3+m_{\mathrm{SS}}b_3)}{M_3}+\frac{m_{\mathrm{SH}}}{M_4}\right], \tag{1}$$

where n_{Si}, n_{Al}, and n_{Na} are the amount of substance of Si, Al, and Na, respectively. M_1, M_2, M_3, and M_4 are the molar masses of SiO_2, Al_2O_3, Na_2O, and NaOH, respectively. m_{MK}, m_{SS}, and m_{SH} are the mix masses of metakaolin, sodium silicate solution, and sodium hydroxide solid, respectively. a_1, a_2, and a_3 are the mass contents of SiO_2, Al_2O_3, and Na_2O in metakaolin, respectively. b_1 and b_3 are the mass contents of SiO_2 and Na_2O in sodium silicate solution, respectively.

This composition of geopolymer had been confirmed to have a good workability and mechanical performance in previous studies (Yan et al., 2016). Geopolymer paste in a blank group (N) was made according to the above ratio without any additive, while the other test groups had specific surfactantsadded. The dosages of surfactants generally ranged from 1 to 20 g/L with reference to the relevant literature (Sarda et al., 2003; Atahan et al., 2008; Kaddami and Pitois, 2019). Therefore, the selected concentration of surfactants was 10 g/L (0.54%, in weight) in a mixed paste to ensure both sufficient addition and simple calculation. For cross comparison, the dosage was kept constant. Details of the proportion of raw materials in the mix are shown in Table 3.

During slurry production, surfactants were first added to the alkali activator solution. The mixed solution (alkaline activator and surfactant) was stirred to the maximum extent of dissolution or dispersion. Then the metakaolin and mixed solution were added to a container in sequence and stirred, at a low speed for 2 min and a high speed for 1 min, using an NJ-160A cement slurry mixer (Wuxi Jianyi Experiment Instrument Co., Ltd., China). Finally, the slurry was poured into cubic molds with 40-mm sides, and was cured at a relative humidity (RH) of >99% and temperature of (20±1) °C for 7 d. Then, the samples were cured at an RH of (50±5)% and temperature of (20±1) °C for 21 d.

2.3 Experimental methods

2.3.1 Viscosity

The viscosity of the slurry (1 min after mixing) was measured using an NDJ-8S digital viscometer (Sithai Experiment Instrument Co., Ltd., China). The viscometer was leveled, and warmed up for 20 min before testing. A No. 4 rotor and 12 r/min starting speed were chosen to measure the viscosity (with the full measurement value range of 0–50 000 mPa·s). During the measurement, each group was tested twice. The difference between the test values and the average value was less than 10%.

Table 3 Mix proportion of raw materials

Mixture	Specific content (g/L)
Metakaolin	666.97
Sodium silicate solution	1066.74
Sodium hydroxide solid	115.27
Surfactant	10.00

Table 2 Group arrangements with different surfactants

Group	Surfactant	Molecular weight (g/mol)	Manufacturer	pH
SLS	Sodium lauryl sulfonate	273	Meryer (Shanghai) Chemical Technology Co., Ltd., China	9.49
APG	Alkyl polyglycoside	348	Karl·Golden (Zhejiang) Biotechnology Co., Ltd., China	12.22
BAC	Benzalkonium chloride	354	Titan (Shanghai) Technology Co., Ltd., China	8.60
SE	Sucrose fatty acid esters	594	Karl·Golden (Zhejiang) Biotechnology Co., Ltd., China	8.15
STA	Stearic acid	284	Dibo (Shanghai) Biotechnology Co., Ltd., China	5.92

2.3.2 Mercury intrusion porosimetry

Mercury intrusion porosimetry (MIP) was performed using an AutoPore IV9500 automatic mercury intrusion meter manufactured by the Micromeritics Instruments Corporation (USA). The analysis range was from 6 nm to 1000 μm. Referring to GB/T 21650.1-2008 (AQSIQ and SAC, 2008), samples were processed into particles of about 3 mm in diameter, and dried at 80 °C for 48 h. Density, porosity, and pore distribution were measured by MIP.

2.3.3 Scanning electron microscopy

SEM was performed using an FEG650 field emission microscope (FEI, USA). SEM was employed to observe microstructural features and analyze micro-area components. The porosity at a certain range was characterized by backscattered electron (BSED) imaging. Six images were taken for each group and the average porosity was calculated. The details of the image analysis process will be discussed in detail below.

During the measurements, the samples were observed in the 20 kV voltage field in a high vacuum environment. Some were cut and dried for porosity observation, and others were cut, polished, and dried for microstructural observation.

2.3.4 Apparent water absorption

Referring to ASTM C642-13 (ASTM, 2013) and GB/T9966-2001 (AQSIQ, 2001), apparent water absorption was measured by the water saturation method. Samples cured for 28 d were washed and dried before weight measurement. Then they were kept in deionized water for 48 h at (21±5) °C. After soaking, the surface of the samples was dried and the saturated mass was weighed and recorded as W. After replacing the water with absolute ethanol for 5 h, samples were dried in an oven at 65 °C for more than 48 h (Ismail et al., 2013a). The weight after drying was obtained and recorded as w_0. The water absorption rate (A) was calculated based on the above parameters as

$$A=\frac{W-w_0}{w_0}\times 100\%. \tag{2}$$

The average value of three samples was taken as the apparent water absorption in each group.

2.3.5 Compressive strength

Referring to GB/T 17671-1999 (SBQTS, 1999), the compressive strength of cubic samples cured for 28 d was measured using an Instron 8802 universal testing machine (UK). A loading speed of 2.4 kN/s was chosen to keep a quasi-static loading process and calculate compressive strength. The average value of six samples from each group was taken as the compressive strength.

3 Results

3.1 Viscosity

The viscosity of slurry is an important index for evaluating the working performance of materials and affects various properties of hardened materials. The slurry of the MKG without surfactant was very sticky with a dynamic viscosity reaching up to 8326 mPa·s. Moreover, as in similar studies (Samson and Cyr, 2018), adding different surfactants increased the viscosity of the slurry to a variable extent. Fig. 4 shows the dynamic viscosity of all groups. Clearly, BAC had the most significant effect on increasing the viscosity, which was 12.11 times as high as in the blank group (N). SLS and APG also had considerable viscosity enhancing effects with a threefold increase. SE and STA improved the viscosity by around 50% compared with the blank group, which can be ignored in comparison to the effect of the other surfactants.

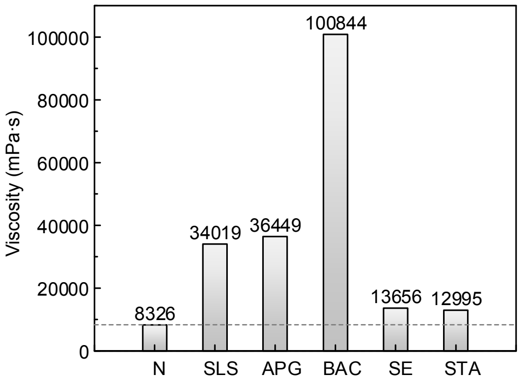

Fig. 4 Dynamic viscosity of MKG slurry after mixing

Microscopically, the extent of viscosity improvement is closely related to the surfactant type, molecular structure, ionic strength, gelatin composition, and ionic strength (Greener et al., 1987; Marchon et al., 2016). APG, BAC, and SLS have large molecular structures with long hydrophobic tails and strong hydrophilic heads (Fig. 3), which increase the crosslinks between hydrocarbon chains of micellar media. Among these three surfactants, BAC, as a cationic surfactant with a hydrophobic benzene ring, is easier to combine with metakaolin particles whose surfaces are negatively charged and aggregated into mass. Although SE and STA have long single chains, the molecular structures of their active ingredients are relatively simple. Their molecular repulsion causes a larger distance between molecules, which significantly inhibits entanglement of hydrocarbon chains. This also indicates that the surfactants SE and STA have good dispersion capability.

The state of the mixing slurry after 1-min standing (Fig. 5) indicates that the generation of bubbles is affected by viscosity. Clearly, the surface has many small bubbles in low viscosity groups, and is smooth in high viscosity groups. Surfactants bound to the metakaolin surface can increase the contact angle, which enhances adsorption of particles on the interfaces, and creates a protective layer to stabilize bubbles (Denkov et al., 1992). The electrostatic repulsion between surfactant layers also contributes to the stabilization of liquid films in foams (Zhao et al., 2004; Feneuil et al., 2017).

The bubbles in the mixture directly affect the microstructure (1 μm–1 mm) of hardened MKG, which is reflected in many physical properties. Therefore, density, apparent water absorption, and compressive strength were tested.

(a) (b) (c)

Fig. 5 Examples of the mixing slurry with different viscosities after 1-min standing

(a) BAC, high viscosity; (b) APG, medium viscosity; (c) Without surfactant, low viscosity

3.2 Density

Fig. 6 shows the bulk density and skeletal density of hardened MKGs measured by MIP. These two kinds of densities are related to porosity, and increase as the total intrusion porosity decreases. The SLS group had the lowest bulk density, 14.50% lower than that of the blank group (N). The bulk density of the APG-group was 9.16% lower than that of the blank group, but changes in the other groups were small and could be ignored. Skeletal density was clearly reduced in the SLS, APG, and SE groups, but showed almost no change in the other groups.

In general, the BAC and STA surfactants had little effect on the density of the MKG, while SLS, APG, and SE reduced the density to some extent. The trends of density and total intrusion porosity were similar, except for the SE group, which showed a noticeable decrease in density but no change in porosity. It is possible that in samples of the SE group a few small pores could not be detected by MIP, and that gel structure was affected. Usually, the geopolymer gel contains not only highly distributed nano-pores, but also aluminosilicate clusters of the order of 5 to 10 nm (Duxson et al., 2005). However, more evidence is needed at nano-scale (1 nm–1 μm) to confirm this phenomenon in further studies.

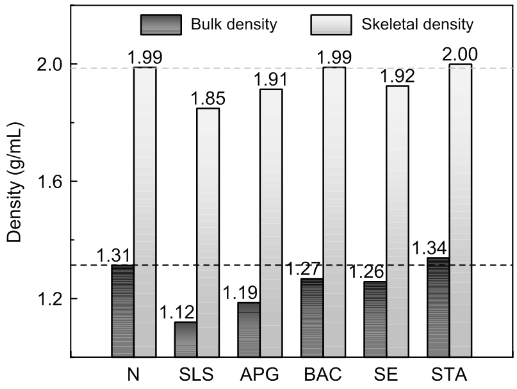

Fig. 6 Bulk density and skeletal density measured by MIP

3.3 Apparent water absorption

Apparent water absorption can characterize the effect of surfactants on the apparent pores of MKGs, and also can reflect the adsorption of surfactant molecules onto the gas-liquid interface system.

Fig. 7 shows the apparent water absorption tested using the water saturation method. SE and STA had almost no effect on apparent water absorption, while SLS, APG, and BAC elevated the absorption with growth rates of 12.15%, 9.39%, and 6.63%, respectively. Like the effect on pores inside (next sections), surfactants can increase or decrease open pores on the surface. Apparent water absorption showed the same trend as total intrusion porosity, in which high porosity led to high apparent water absorption. This result is consistent with previous studies (Borges et al., 2016; Mobili et al., 2016). Compared with the change of apparent pores, the effect caused by surfactants in pore solution can be ignored. In addition to porosity, defects in samples of the SLS, APG, and BAC groups probably increased the number of tunnels, which enhanced capillary absorption. Water absorption indirectly represents the distribution of apparent pores, as a pore characteristic. The details of porosity and pore distribution characterized by MIP and SEM were analyzed to verify the consistency of the MKG microstructure.

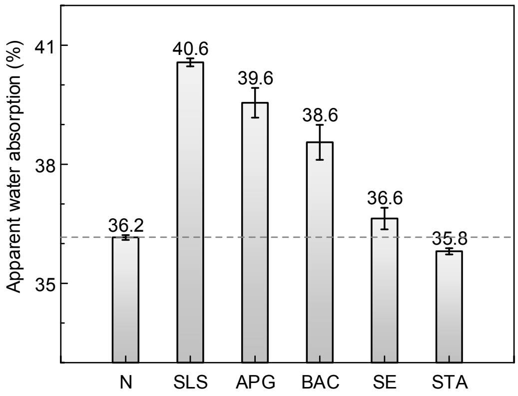

Fig. 7 Apparent water absorption tested by water saturation method

3.4 Compressive strength

The mechanical properties of MKGs are affected by microstructure and macro-defects to a certain extent. Generally, MKGs have a high compressive strength due mainly to the formation of gel structures with a strong load (Shi et al., 2006). Fig. 8 shows that the compressive strength of all samples, except STA, decreased after surfactants were added. The trend of compressive strength is consistent with the total intrusion porosity, and with results from other studies (Park et al., 2016). It results mainly from the decrease in compactness, and the capability to change bonding. Slipping of the raw materials and the gels caused by surfactants is also a significant contributing factor.

Only samples from the STA group showed increased compressive strength (by 5.16%). This results mainly from their low porosity, homogeneous gels, and dense microstructure due to full geopolymerization. Samples from the SLS and APG groups had the lowest compressive strength, reduced by 21.08% and 30.04%, respectively. With the addition of SLS or APG, the porosity greatly increased, and the microstructure became looser. In particular, APG had the capacity to promote the generation of macro-pores, leading to the lowest compressive strength (Farhana et al., 2013). The lubricating effect of clustered APG molecules was also an important factor reducing compressive strength. Samples of BAC and SE showed smaller reductions of 13.45% and 9.19%, respectively. Although they had a denser gel structure and fewer defects, their strength was still lower than that of the blank group. For the BAC group, which had the highest viscosity, more micron-scale bubbles caused the lower ultimate compressive strength. The surfactants may also have had an impact on the connection between the clusters of raw materials and the gel clusters. Surfactants adsorbing on the surface of the particles generate repulsive forces and block some parts of the adhesion, probably causing direct relative slip of the clusters.

Mechanical properties are of great significance for evaluating the value of applying surfactants to geopolymers. To explore the mechanisms of action of surfactants at micro scale, we observed and analyzed the microstructures.

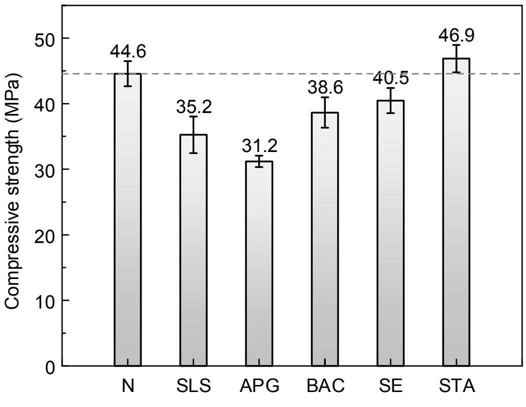

Fig. 8 Compressive strength measured by the universal testing machine

3.5 Microstructure analyses

Micro-defects are an important indicator for evaluating the microstructure of MKGs and can to some extent determine their physical properties. Fig. 9 shows the secondary electron images (ETD) of the microstructures in magnification of 20000.

Compared with the blank group, there were many more micro-defects in samples from the SLS and APG groups than in those from the BAC, SE, and STA groups. In the blank group, there were many narrow micro-cracks running in different directions. After adding SLS or APG, more defects of unreacted metakaolin appeared in different forms. In the SLS group, metakaolin particles were interlaced and the micro-cracks were jagged. In the APG group, the layers were well-ordered and the micro-cracks were long and wide and ran in similar directions. In the APG group, several closed global bubble pores with a diameter of about 200 nm were found. This was probably due to APG introducing stable and dispersed micro-bubbles smaller than 1 μm. The BAC group had fewer defects that were composed of neatly arranged pieces of unreacted metakaolin. The microstructure of the STA and SE groups was the densest, with a uniform gel and few defects.

To further describe the effects of surfactants on the compactness of the MKG, the porosity and pore distribution observed through MIP and SEM were analyzed. The mechanism by which the surfactants affected the microstructure will be discussed in detail.

3.6 Porosity characterization

MIP is widely used to calculate the porosity, pore distribution, and other parameters of cement-based materials. As shown in the schematic representation in Fig. 10, materials contain two types of pore connections: (a) a fine pore connected to the exterior of the sample through a large pore; (b) a large pore connected to the exterior of the sample through a fine pore. For the first type, the Washburn equation model provides a correct tally of volume versus pore diameter (Diamond, 2000). However, for the second type, the result tested by MIP is somewhat biased. The large pores are intruded when they reach the threshold pressure of the connecting fine pores. All of the volume is recorded as the fine pore volume, and the existence of the large pores is undetected (Diamond, 2000). This bias is called the ‘ink bottle’ effect (Szekely et al., 1971). Geopolymer is a material with a large number of pores (Zuda et al., 2008), and the pore diameter is concentrated mainly in the range from 5 to 50 nm (Rovnaník, 2010; Provis and van Deventer, 2013). As a result, its porosity in different ranges obtained by MIP is greatly affected by the ‘ink bottle’ effect. Although the MIP technique has its limitations in the characterization of total porosity, it is still useful for providing threshold diameters and intrudable pore space measurements of pores from 6 nm to 1000 μm (Diamond, 2000). The total intrusion porosity measured by MIP has a significant effect on the mechanical properties and durability of MKGs. The bubbles and pores in the SEM images are also connected and intrinsic. The total intrusion porosity still serves as a significant comparative index for the capacity of pore systems.

To weaken the impact of the ‘ink bottle’ effect, researchers have applied the MIP method and image analysis to characterize the porosity of cementing material (Abell et al., 1999; Romero and Simms, 2008). In this study, the porosity obtained through MIP and SEM (Fig. 11) was combined to give an accurate comparison of pore distribution. The pores were divided into three ranges: large pores ($d\geq$ 20 μm), medium pores (150 nm$\leq d<$20 μm), and small pores (6 nm$\leq d<$150 nm).

Fig. 12 is an illustrative diagram of BSED image analysis in different diameter ranges. Based on the color order histogram of each raw image, the point with a slope k of tan45° (k=1) was regarded as the threshold point for binarization, which was consistent with a manual check of the pores. The pixels with a gray value lower than the threshold were set to 0, while others were set to 255 after binarization, and clear black and white images were obtained. The pixels of pores were counted by the image analysis program and checked manually to ensure that all pores were identified. The identified pixels of bubbles, pores, and cracks were black, and bubbles and pores were highlighted in yellow. The detailed porosity calculation process was as follows:

1. In the BSED images in magnification of 100, the discernable inner diameters of bubble pores and defects were larger than 20 μm. These pores were denoted as large pores, and the porosity (Φ_{L}) was calculated as

$$\Phi_{\mathrm{L}}=\frac{S_1}{S_1+S_2}, \tag{3}$$

where S_1 is the pixel value of bubble pores and S_2 is the pixel value of the MKG matrix in magnification of 100.

2. In the BSED images with magnification of 2000, pores with diameters from 150 nm to 20 μm were denoted as medium pores, and the porosity (Φ_{M}) was calculated as

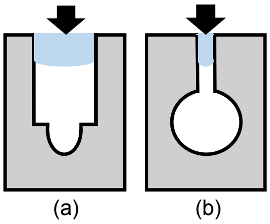

Fig. 10 Schematic representation of two types of pore connections in materials

(a) A fine pore connected to the exterior of the sample through a large pore; (b) A large pore connected to the exterior of the sample through a fine pore

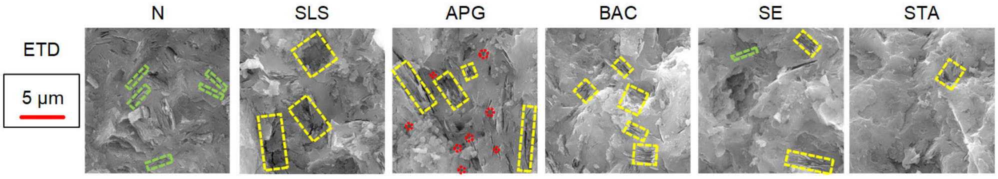

Fig. 9 ETD images of the microstructures observed using SEM

The ETD images show the micron-scale microstructure in magnification of 20000 of samples from different groups. Green boxes indicate the micro-cracks; yellow boxes indicate defects of unreacted metakaolin; red boxes indicate unconnected global bubble pores

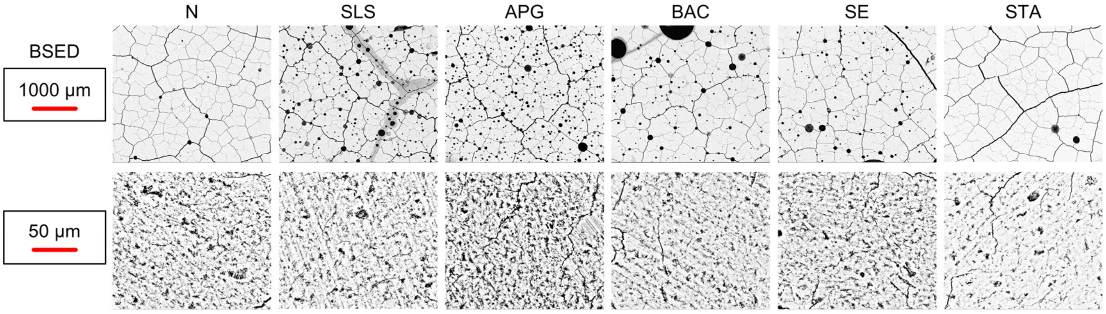

Fig. 11 BSED images of large- and medium-sized pores observed using SEM

The first row of BSED images were in magnification of 100, and bubble pores larger than 20 μm can be counted. The second row of BSED images were in magnification of 2000, and pores with a diameter from 150 nm to 20 μm can be counted

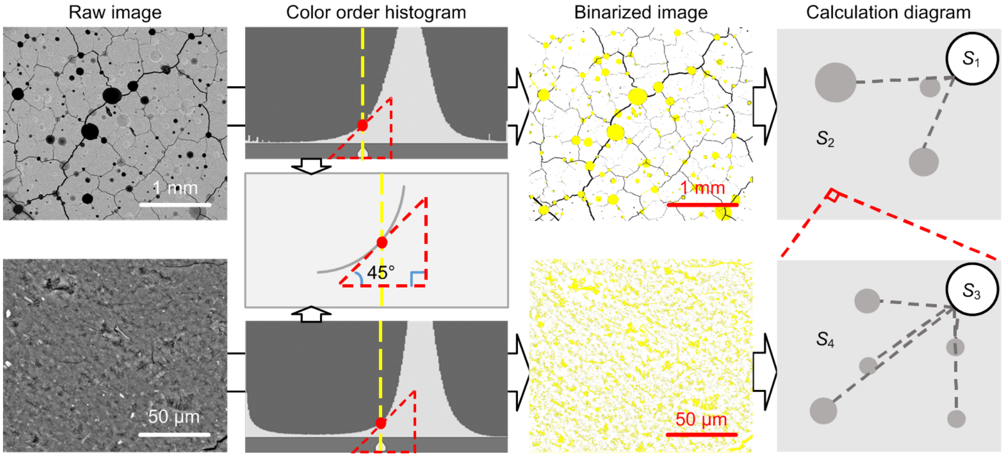

Fig. 12 Illustrative diagram of BSED image analysis and the porosity calculation process in different diameter ranges

Pores and defects in different diameter ranges are observed by SEM in raw images. Based on color order histogram analysis and image binarization, pore distribution and porosity can be calculated using pixels

$$\Phi_{\mathrm{M}} = \frac{S_2 S_3}{(S_1 + S_2)(S_3 + S_4)}, \tag{4}$$

where S_3 is the pixel value of the pores and S_4 is the pixel value of the MKG matrix in magnification of 2000.

3. MIP directly measures the total intrusion porosity (Φ_{T}) within the measuring range of the samples. The porosity (Φ_{S}) of the small pores with diameters from 6 to 150 nm was calculated as

$$\Phi_{\mathrm{S}} = \Phi_{\mathrm{T}} - \Phi_{\mathrm{M}} - \Phi_{\mathrm{L}}. \tag{5}$$

4. Cracks in the view were due mainly to inevitable high-level vacuum drying before the SEM observation (Ismail et al., 2013a). Their presence is method-dependent rather than material-dependent, which is beyond the scope of this paper. Thus, these cracks were not included in the calculation and discussion.

Fig. 13 demonstrates the porosity characterized by SEM and MIP. The order of the groups is in accordance with their total intrusion porosity from high to low. Clearly, all the surfactants, except STA, increased the total intrusion porosity to some extent.

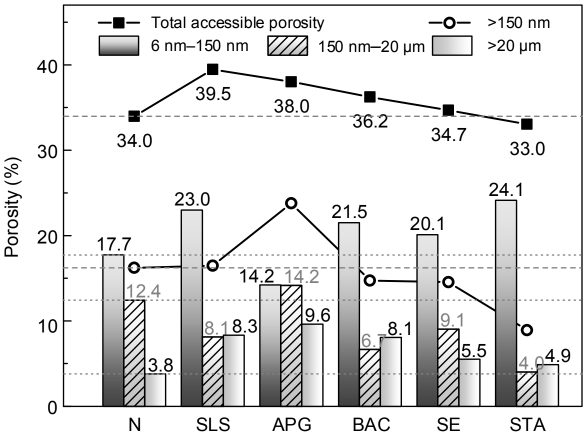

Fig. 13 Porosity of different diameter ranges characterized by SEM and MIP

Small pores with diameters from 6 to 150 nm were the most common among the three ranges mentioned above. The pores in this range include some gel pores (d<10 nm) and capillary pores (10 nm≤d≤1000 nm), which come mainly from the porous amorphous phase and geopolymerization of the system (Bose and Saha, 2003). In regard to the porosity of small pores, the APG group was the only group that showed a decline, of 19.77%, while the other groups all showed an increase compared with the blank group. The biggest improvement, of 36.16%, occurred in the STA group. This indicates that most surfactants can promote the generation of gels, and the pore size becomes smaller. The threshold diameter increased by about 10 nm only with the addition of SLS, and increased less than 5 nm with the addition of the other surfactants. The nano-scale pores were distributed within a range instead of being concentrated on a certain pore size in the different groups (Fig. 14).

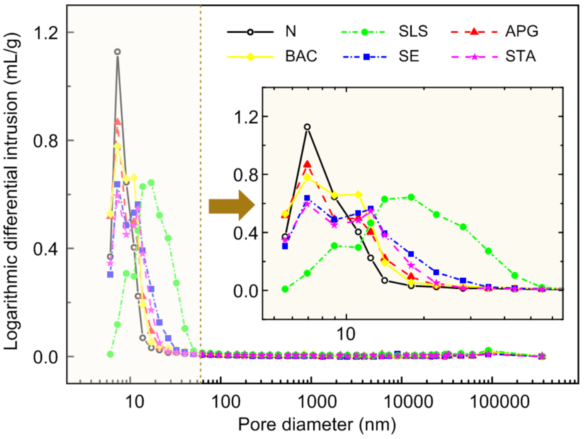

Fig. 14 Pore distribution obtained by MIP

The distribution of pores with diameters within the range from 5 to 60 nm are shown in the chart inset on the right

For medium pores with diameters ranging from 150 nm to 20 μm, most of the capillary pores and small bubbles were included in the range. Except for the APG group, the porosity decreased, especially the porosity of the STA group, which was only 32.26% of that of the blank group. Studies have shown that porosity and threshold pore size affect the permeability of materials (Garboczi, 1990; Ma et al., 2013). Therefore, it is important to control the porosity in this range in geopolymers which contain a large number of micron-pores.

For large pores with diameters of more than 20 μm, the porosity of all groups increased compared with the blank group. The APG, SLS, and BAC groups showed the largest increases, with porosities 2.53, 2.18, and 2.13 times that of the blank group, respectively. The porosity of the STA group increased slightly. Pores in this range are composed mainly of bubbles, which originate from entrapped air (Du and

Folliard, 2005; Cantat et al., 2013), and the interface space between metakaolin particles and gels (Rodríguez et al., 2013).

Different surfactants had different effects on pores of different sizes. In general, SLS and APG led to higher porosity, looser microstructures, and more micro-defects for a relatively low level of geopolymerization. BAC led to a denser pore structure with smaller pores. Both SE and STA led to a relatively low porosity and dense microstructures for more complete geopolymerization. Therefore, understanding the mechanisms of action of surfactants at the level of molecular interaction is of great significance for their application in the field of geopolymers. In the next section, the mechanisms underlying the adsorption of surfactants will be proposed to further explain their effects on MKGs.

4 Discussion

4.1 Surfactant adsorption capacities

Generally, surfactants can adsorb onto solid-liquid interfaces, or self-associate into micelles or liquid crystals (Marchon et al., 2016). Like other inorganic salts and oxides, metakaolin has a high surface energy which leads to strong adsorbability (Andrejkovičová et al., 2016). Thus, surfactants with different molecular structures can adsorb onto the surface of metakaolin particles in various configurations (Partyka et al., 1984; Marchon et al., 2016). On the hydrophilic surface of metakaolin, the main reason for adsorption is different for ionic and nonionic surfactants. For ionic surfactants, adsorption behavior is governed by the charge of the surface and counter ions present in the electrolytes (Tadros, 2005). For nonionic surfactants, it can be driven by hydrogen bonding of the polar moieties (hydrophilic heads) (Nicoleau et al., 2014). The adsorption capacities of the five surfactants were compared with the following results:

1. The cationic surfactant BAC had the strongest adsorption capacity. The surface of metakaolin is negatively charged in alkaline conditions. According to the model of a modified double-electrical layer proposed by Grahame (1947), water film connecting with the surface of particles is divided into two layers: an inner layer with adsorbed cations and an outer layer with adsorbed anions (Konan et al., 2009). Therefore, the hydrophilic heads of the anionic surfactants SLS and STA exist in the outer layer, while the hydrophilic heads of the cationic surfactant BAC are bonded in the inner layer. Saleh et al. (2014) proved that nitrogen is easily adsorbed under certain conditions, which can further promote the adsorption capacity of BAC.

2. For anionic surfactants, adsorption of SLS was weaker than that of STA and SE. According to the theory of electronegativity proposed by Pauling (1949), the acidity of sulfonic acid is stronger than that of carboxylic acid, so the sulfonates ($R\text{-}SO_3^-$, SLS) have a weaker ability to attract positive charge than the carboxylates ($R\text{-}COO^-$, STA and SE). Therefore, we conclude that the adsorption capacity of SLS is weaker than that of STA and SE.

3. The effective adsorption of STA is stronger than that of SE. Though the active ingredient is stearic acid ($CH_3\text{-}(CH)_{16}\text{-}COO^-$) in both the STA and SE groups, the adsorption is different. There are free hydrophilic heads in the SE group, which compete for the adsorption site on the metakaolin surface (Marchon et al., 2016), resulting in a stronger adsorption of STA than that of SE.

4. The nonionic surfactant APG had the weakest adsorption capacity. Generally, ionic bonds have a much stronger force than hydrogen bonds (van der Waals forces). Consequently, the adsorption of the nonionic surfactant APG on the metakaolin surface was the weakest, and could even lead to ineffective adsorption.

5. The adsorption capacities of the five surfactants ordered from the strongest to weakest were: BAC>STA>SE>SLS>APG.

4.2 Microstructure effects

Like cement material (Uchikawa et al., 1992; Du and Folliard, 2005), the geopolymerization and microstructure of MKGs are affected by different surfactant adsorption capacities. As shown in the schematic representation (Fig. 15), the five kinds of surfactants were adsorbed onto the surface of metakaolin particles to variable degrees, and could be divided into two types based on their looser or denser microstructure. Compared to micron-scale metakaolin particles (average particle diameter of 5.91 μm), nano-scale surfactant molecules can, theoretically, enter between the layers, and this may also be affected by the size, configuration, and adsorption capacity of molecules.

Based on the adsorption mechanisms shown in Fig. 15, the surfactants SLS and APG can lead to looser microstructures. Their molecules are less readily adsorbed onto the surface of metakaolin because of their relatively weak adsorption. A large number of molecules are held together and self-associate into micelles by their long hydrophobic tails, making it harder for them to enter the gaps between metakaolin particles. Therefore, the metakaolin cannot be well dispersed and in good contact with the activator, which leads to relatively low level of geopolymerization. A small number of aggregated surfactant molecules enter the gaps, which causes disorderly slip between metakaolin particles which leads to more micro-defects.

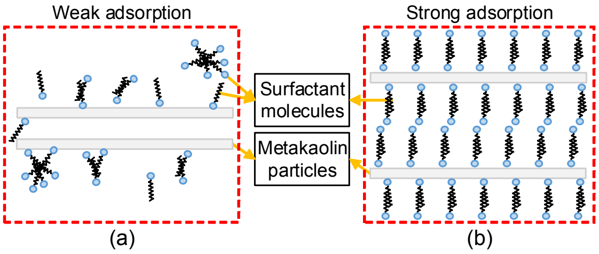

Fig. 15 Schematic representation of the connection between surfactant molecules and metakaolin particles: (a) SLS, APG; (b) BAC, SE, and STA

It is harder for molecules of SLS and APG to adsorb onto the surface of metakaolin, but they self-associate into micelles, making it harder for them to enter the gaps between metakaolin particles. BAC, SE, and STA molecules are more easily adsorbed onto the surface of metakaolin, and effectively disperse metakaolin particles

The SLS surfactant resulted in obvious massive defects at the micron-scale. Some molecules are free, and some adsorb onto the metakaolin surface to crosslink with cluster-forming molecules. This adsorption behavior leads to disorderly slip between metakaolin particles, which causes more chaotic and shorter micro-cracks. APG, as a non-ion surfactant, has a large hydrophilic head with hydroxyl and ether groups which can form multiple hydrogen bonds with oxygen in metakaolin (Konan et al., 2009). However, the weak adsorption capacity and large molecular volume prevent APG from being evenly distributed on the surface, and promote the formation of more molecular clusters. This causes lateral displacement of layers to accommodate the clusters, leading to long micro-cracks. Furthermore, APG is probably easier to wrap on clusters of multilayer metakaolin to block the geopolymerization, and causes a loose and heterogeneous structure due to the strong intermolecular forces.

The surfactants BAC, SE, and STA led to denser microstructures. They have stronger adsorption capacities which makes them bond to the metakaolin surface uniformly and firmly. These surfactants lead to steric repulsion between grains, which is beneficial for dispersing the metakaolin particles (Flatt and Schober, 2012). They can efficiently promote the geopolymerization of metakaolin, and lead to denser gels and fewer defects (Saleh et al., 2018).

BAC can make pores smaller and leads to a denser pore structure. As a cationic surfactant, the hydrophilic head of BAC can be strongly fixed at the inner layer of the water film due to the ionic bond. Thus, BAC can effectively disperse metakaolin particles to promote geopolymerization. The relatively free hydrophobic groups, including carbon chains and benzene rings, can promote crosslinking and coupling between molecules, leading to the orderly arrangement of metakaolin particles (Fig. 9). However, the compressive strength of samples from the BAC group was still lower than that of the blank group. This results mainly from the presence of more micron-scale bubbles due to the high viscosity. Therefore, the effect of surfactants on mechanical properties needs a comprehensive consideration of defects, pore distribution, microstructure, and geopolymerization.

SE and STA led to the densest gel structure. Most of surfactant molecules adsorb onto the surface of particles, which makes the raw materials distribute evenly due to mutual exclusion of charges and cross-linking of the long carbon chain. The dispersion of metakaolin provides ample reaction space for more complete geopolymerization. Previous studies have proved that hydrophilic groups can be deprotonated at the elevated pH of these systems (Labbez et al., 2006; Nicoleau et al., 2014; Adio et al., 2017), which explains once again why samples of the STA group (the only acidic aqueous solution) had the densest structure.

4.3 Bubble formation

Surfactants have a high affinity for liquid-air interfaces which affects the formation of bubbles (Marchon et al., 2016). The dynamics of surfactant adsorption is faster than surface formation at the air-water interface, which guarantees the creation of an interface (Cantat et al., 2013). Adsorbed surfactants result in a lowering of surface tension, so less energy is needed to generate stable bubbles. Surfactants adsorbing on both sides of a water film also cause steric interactions, making bubbles repel each other, resulting in large pores in MKGs (Feneuil et al., 2017). APG has six hydrophilic groups including a hydroxyl and an ether group (Fig. 3), which stabilize its attachment to the water film. The hydrophilic head of SLS has a large molecular weight, and the hydrophobic part of BAC has a unique benzene ring (Fig. 3). Electrostatic interaction resulting from ionic surfactants such as SLS and BAC also can contribute to the stabilization of bubbles (Feneuil et al., 2017). The effective components offered by SE and STA are the same, and have relatively smaller steric interactions.

5 Conclusions

Surfactants with specific molecular configurations affect the physical properties and microstructure of MKGs. All surfactants can increase the slurry viscosity and promote the generation of bubbles. BAC has the strongest capacity to increase viscosity, and APG the strongest capacity to produce bubbles. The trends of density, water absorption, and compressive strength are related to the total intrusion porosity, which reflects the consistency of the microscopic and macroscopic, external and internal structures of MKGs.

SLS and APG lead to a higher porosity, looser microstructure, and more micro-defects for the clustered molecules due to their weaker adsorption. BAC, SE, and STA lead to a relatively lower porosity and denser microstructure for better geopolymerization, resulting from the stronger adsorption. Based on the experimental results, the mechanisms underlying surfactant adsorption on the surface of metakaolin are proposed, and suggest that stronger adsorption leads to a denser microstructure.

The specific effects of the five surfactants on MKG were as follows:

1. SLS is an anion surfactant with a relatively weak adsorption to metakaolin. It can not only greatly increase the total intrusion porosity, but also promote the development of small pores into large pores. Its loose microstructure leads to a low density and compressive strength, and the highest apparent water adsorption.

2. APG is a non-ion surfactant with a large hydrophilic head which exists between metakaolin particles mainly in the form of micelles. It can increase the total intrusion porosity. In particular, the pores larger than 150 nm had 2.53 times the porosity of samples from the blank group. Another outstanding feature of APG is that it can accelerate the creation of bubble pores due to its relatively high viscosity. Samples from the APG group had high apparent water absorption and low density. The lowest compressive strength was found in the APG group, mainly because of micro-defects.

3. BAC is a cationic surfactant containing a hydrophobic benzene ring and a long carbon chain. It was not only firmly integrated in the metakaolin, but also led to strong coupling between molecules. BAC had only a slight impact on total intrusion porosity, apparent water absorption, and compressive strength. It is an effective and suitable thickener. Its viscosity was 12.11 times as high as that of the geopolymer slurry without an additive.

4. SE and STA are both anion surfactants whose molecules are readily adsorbed on the surface of metakaolin. These two surfactants developed the densest microstructure and promoted a change from larger to smaller pores. Their effects on the viscosity and total intrusion porosity were almost negligible. The relative density of SE was reduced, suggesting that there were a number of closed pores. STA increased compressive strength because of its denser microstructure and gels.

This study was a preliminary experimental investigation of the use of surfactants to adjust the microstructure and properties of geopolymer materials. The results showed that the molecular adsorption capability of surfactants plays an important role in forming geopolymer binder structures. However, further studies considering the interaction between the chemical additives and geopolymer gels are needed. A deeper examination of the mechanisms by which chemically bonded molecules influence the polymerization processes of geopolymers would also be valuable.

Contributors

Dong-ming YAN and Yi LIU were the principal investigator (PI) and co-PI of this project, respectively. Dong-ming YAN was also involved in preparing the manuscript. Sheng-qian RUAN and Shi-kun CHEN conducted the experiments and processed the test data. Ye TIAN, Hai-long WANG, and Tian-nan YE revised and edited the manuscript.

Conflict of interest

Dong-ming YAN, Sheng-qian RUAN, Shi-kun CHEN, Yi LIU, Ye TIAN, Hai-long WANG, and Tian-nan YE declare that they have no conflict of interest.

References

Abell AB, Willis KL, Lange DA, 1999. Mercury intrusion porosimetry and image analysis of cement-based materials. *Journal of Colloid and Interface Science*, 211(1): 39-44.
https://doi.org/10.1006/jcis.1998.5986

Adio SO, Omar MH, Asif M, et al., 2017. Arsenic and selenium removal from water using biosynthesized nanoscale zero-valent iron: a factorial design analysis. *Process Safety and Environmental Protection*, 107:518-527.
https://doi.org/10.1016/j.psep.2017.03.004

Andrejkovičová S, Sudagar A, Rocha J, et al., 2016. The effect of natural zeolite on microstructure, mechanical and heavy metals adsorption properties of metakaolin based geopolymers. *Applied Clay Science*, 126:141-152.
https://doi.org/10.1016/j.clay.2016.03.009

AQSIQ (General Administration of Quality Supervision, Inspection and Quarantine), 2001. Test Methods for Natural Facing Stones, GB/T9966-2001. National Standards of the People's Republic of China (in Chinese).

AQSIQ (General Administration of Quality Supervision, Inspection and Quarantine) and SAC (Standardization Administration), 2008. Pore Size Distribution and Porosity of Solid Materials by Mercury Porosimetry and Gas Adsorption-Part 1: Mercury Porosimetry, GB/T 21650.1-2008. National Standards of the People's Republic of China (in Chinese).

ASTM (American Society of Testing Materials), 2013. Standard Test Method for Density, Absorption, and Voids in Hardened Concrete, ASTM C642-13. National Standards of USA.
http://www.astm.org/cgi-bin/resolver.cgi?C642

Atahan HN, Carlos Jr C, Chae S, et al., 2008. The morphology of entrained air voids in hardened cement paste generated with different anionic surfactants. *Cement and Concrete Composites*, 30(7):566-575.
https://doi.org/10.1016/j.cemconcomp.2008.02.003

Bai CY, Colombo P, 2017. High-porosity geopolymer membrane supports by peroxide route with the addition of egg white as surfactant. *Ceramics International*, 43(2):2267-2273.
https://doi.org/10.1016/j.ceramint.2016.10.205

Bai CY, Ni T, Wang QL, et al., 2018. Porosity, mechanical and insulating properties of geopolymer foams using vegetable oil as the stabilizing agent. *Journal of the European Ceramic Society*, 38(2):799-805.
https://doi.org/10.1016/j.jeurceramsoc.2017.09.021

Baščarević Z, Komljenović M, Miladinović Z, et al., 2013. Effects of the concentrated NH_4NO_3 solution on mechanical properties and structure of the fly ash based geopolymers. *Construction and Building Materials*, 41: 570-579.
https://doi.org/10.1016/j.conbuildmat.2012.12.067

Borges PHR, Banthia N, Alcamand HA, et al., 2016. Performance of blended metakaolin/blastfurnace slag alkali-activated mortars. *Cement and Concrete Composites*, 71: 42-52.
https://doi.org/10.1016/j.cemconcomp.2016.04.008

Bose S, Saha SK, 2003. Synthesis and characterization of hydroxyapatite nanopowders by emulsion technique. *Chemistry of Materials*, 15(23):4464-4469.
https://doi.org/10.1021/cm0303437

Brylewska K, Rożek P, Król M, et al., 2018. The influence of dealumination/desilication on structural properties of metakaolin-based geopolymers. *Ceramics International*, 44(11):12853-12861.
https://doi.org/10.1016/j.ceramint.2018.04.095

Cantat I, Cohen-Addad S, Elias F, et al., 2013. Foams: Structure and Dynamics. Oxford University Press, New York, USA.

Cilla MS, Morelli MR, Colombo P, 2014. Effect of process parameters on the physical properties of porous geopolymers obtained by gelcasting. *Ceramics International*, 40(8):13585-13590.
https://doi.org/10.1016/j.ceramint.2014.05.074

Curosu I, Liebscher M, Mechtcherine V, et al., 2017. Tensile behavior of high-strength strain-hardening cement-based composites (HS-SHCC) made with high-performance polyethylene, aramid and PBO fibers. *Cement and Concrete Research*, 98:71-81.
https://doi.org/10.1016/j.cemconres.2017.04.004

Denkov ND, Ivanov IB, Kralchevsky PA, et al., 1992. A possible mechanism of stabilization of emulsions by solid particles. *Journal of Colloid and Interface Science*, 150(2):589-593.
https://doi.org/10.1016/0021-9797(92)90228-E

Diamond S, 2000. Mercury porosimetry: an inappropriate method for the measurement of pore size distributions in cement-based materials. *Cement and Concrete Research*, 30(10):1517-1525.
https://doi.org/10.1016/S0008-8846(00)00370-7

Du LX, Folliard KJ, 2005. Mechanisms of air entrainment in concrete. *Cement and Concrete Research*, 35(8):1463-1471. https://doi.org/10.1016/j.cemconres.2004.07.026

Duan P, Yan CJ, Zhou W, et al., 2016. Fresh properties, mechanical strength and microstructure of fly ash geopolymer paste reinforced with sawdust. *Construction and Building Materials*, 111:600-610. https://doi.org/10.1016/j.conbuildmat.2016.02.091

Duxson P, Provis JL, Lukey GC, et al., 2005. Understanding the relationship between geopolymer composition, microstructure and mechanical properties. *Colloids and Surfaces A: Physicochemical and Engineering Aspects*, 269(1-3):47-58. https://doi.org/10.1016/j.colsurfa.2005.06.060

Duxson P, Fernández-Jiménez A, Provis JL, et al., 2007a. Geopolymer technology: the current state of the art. *Journal of Materials Science*, 42(9):2917-2933. https://doi.org/10.1007/s10853-006-0637-z

Duxson P, Provis JL, Lukey GC, et al., 2007b. The role of inorganic polymer technology in the development of ‘green concrete’. *Cement and Concrete Research*, 37(12): 1590-1597. https://doi.org/10.1016/j.cemconres.2007.08.018

El-Naggar MR, El-Dessouky MI, 2017. Re-use of waste glass in improving properties of metakaolin-based geopolymers: mechanical and microstructure examinations. *Construction and Building Materials*, 132:543-555. https://doi.org/10.1016/j.conbuildmat.2016.12.023

Farhana ZF, Kamarudin H, Rahmat A, et al., 2013. A study on relationship between porosity and compressive strength for geopolymer paste. *Key Engineering Materials*, 594-595:1112-1116. https://doi.org/10.4028/www.scientific.net/kem.594-595.1112

Feneuil B, Pitois O, Roussel N, 2017. Effect of surfactants on the yield stress of cement paste. *Cement and Concrete Research*, 100:32-39. https://doi.org/10.1016/j.cemconres.2017.04.015

Flatt R, Schober I, 2012. Superplasticizers and the rheology of concrete. *In*: Roussel N (Ed.), Understanding the Rheology of Concrete. Woodhead Publishing, Cambridge, UK, p.144-208. https://doi.org/10.1533/9780857095282.2.144

Garboczi EJ, 1990. Permeability, diffusivity, and microstructural parameters: a critical review. *Cement and Concrete Research*, 20(4):591-601. https://doi.org/10.1016/0008-8846(90)90101-3

Grahame DC, 1947. The electrical double layer and the theory of electrocapillarity. *Chemical Reviews*, 41(3):441-501. https://doi.org/10.1021/cr60130a002

Greener J, Contestable BA, Bale MD, 1987. Interaction of anionic surfactants with gelatin: viscosity effects. *Macromolecules*, 20(10):2490-2498. https://doi.org/10.1021/ma00176a029

He S, Qiu JS, Li JX, et al., 2017. Strain hardening ultra-high performance concrete (SHUHPC) incorporating CNF-coated polyethylene fibers. *Cement and Concrete Research*, 98:50-60. https://doi.org/10.1016/j.cemconres.2017.04.003

Ismail I, Bernal SA, Provis JL, et al., 2013a. Drying-induced changes in the structure of alkali-activated pastes. *Journal of Materials Science*, 48(9):3566-3577. https://doi.org/10.1007/s10853-013-7152-9

Ismail I, Bernal SA, Provis JL, et al., 2013b. Influence of fly ash on the water and chloride permeability of alkali-activated slag mortars and concretes. *Construction and Building Materials*, 48:1187-1201. https://doi.org/10.1016/j.conbuildmat.2013.07.106

Kaddami A, Pitois O, 2019. A physical approach towards controlling the microstructure of metakaolin-based geopolymer foams. *Cement and Concrete Research*, 124: 105807. https://doi.org/10.1016/j.cemconres.2019.105807

Konan KL, Peyratout C, Smith A, et al., 2009. Comparison of surface properties between kaolin and metakaolin in concentrated lime solutions. *Journal of Colloid and Interface Science*, 339(1):103-109. https://doi.org/10.1016/j.jcis.2009.07.019

Kong DLY, Sanjayan JG, Sagoe-Crentsil K, 2007. Comparative performance of geopolymers made with metakaolin and fly ash after exposure to elevated temperatures. *Cement and Concrete Research*, 37(12):1583-1589. https://doi.org/10.1016/j.cemconres.2007.08.021

Kong DLY, Sanjayan JG, Sagoe-Crentsil K, 2008. Factors affecting the performance of metakaolin geopolymers exposed to elevated temperatures. *Journal of Materials Science*, 43(3):824-831. https://doi.org/10.1007/s10853-007-2205-6

Kriven WM, Bell JL, Gordon M, 2006. Microstructure and microchemistry of fully-reacted geopolymers and geopolymer matrix composites. *In*: Bansal NP, Singh JP, Kriven WM, et al. (Eds.), Advances in Ceramic Matrix Composites IX. American Ceramic Society, Westerville, USA, p.227-250. https://doi.org/10.1002/9781118406892.ch15

Külaots I, Hsu A, Hurt RH, et al., 2003. Adsorption of surfactants on unburned carbon in fly ash and development of a standardized foam index test. *Cement and Concrete Research*, 33(12):2091-2099. https://doi.org/10.1016/S0008-8846(03)00232-1

Labbez C, Jönsson B, Pochard I, et al., 2006. Surface charge density and electrokinetic potential of highly charged minerals: experiments and Monte Carlo simulations on calcium silicate hydrate. *The Journal of Physical Chemistry B*, 110(18):9219-9230. https://doi.org/10.1021/jp057096+

Lee WKW, van Deventer JSJ, 2002. The effect of ionic contaminants on the early-age properties of alkali-activated fly ash-based cements. *Cement and Concrete Research*, 32(4):577-584. https://doi.org/10.1016/S0008-8846(01)00724-4

Lyon RE, Balaguru PN, Foden A, et al., 1997. Fire-resistant

aluminosilicate composites. *Fire and Materials*, 21(2): 67-73.
https://doi.org/10.1002/(SICI)1099-1018(199703)21:2<67::AID-FAM596>3.0.CO;2-N

Ma Y, Hu J, Ye G, 2013. The pore structure and permeability of alkali activated fly ash. *Fuel*, 104:771-780.
https://doi.org/10.1016/j.fuel.2012.05.034

MacLeod AJN, Collins FG, Duan WH, et al., 2019. Quantitative microstructural characterisation of Portland cement -carbon nanotube composites using electron and X-ray microscopy. *Cement and Concrete Research*, 123: 105767.
https://doi.org/10.1016/j.cemconres.2019.05.012

Marchon D, Mantellato S, Eberhardt AB, et al., 2016. Adsorption of chemical admixtures. *In*: Aïtcin PC, Flatt RJ (Eds.), Science and Technology of Concrete Admixtures. Woodhead Publishing, Cambridge, UK, p.219-256.
https://doi.org/10.1016/B978-0-08-100693-1.00010-2

Masi G, Rickard WDA, Vickers L, et al., 2014. A comparison between different foaming methods for the synthesis of light weight geopolymers. *Ceramics International*, 40(9): 13891-13902.
https://doi.org/10.1016/j.ceramint.2014.05.108

Mobili A, Belli A, Giosuè C, et al., 2016. Metakaolin and fly ash alkali-activated mortars compared with cementitious mortars at the same strength class. *Cement and Concrete Research*, 88:198-210.
https://doi.org/10.1016/j.cemconres.2016.07.004

Morsy MS, Alsayed SH, Al-Salloum Y, et al., 2014. Effect of sodium silicate to sodium hydroxide ratios on strength and microstructure of fly ash geopolymer binder. *Arabian Journal for Science and Engineering*, 39(6):4333-4339.
https://doi.org/10.1007/s13369-014-1093-8

Mulligan CN, Yong RN, Gibbs BF, 2001. Surfactant-enhanced remediation of contaminated soil: a review. *Engineering Geology*, 60(1-4):371-380.
https://doi.org/10.1016/S0013-7952(00)00117-4

Naden BJ, 2016. Competitive adsorption of surfactant foaming agents to nanoclays added to cement foams for enhanced strength. *Materials and Structures*, 49(5):1667-1675.
https://doi.org/10.1617/s1152

Nasvi MCM, Ranjith PG, Sanjayan J, 2014. A numerical study of CO_2 flow through geopolymer under down-hole stress conditions: application for CO_2 sequestration wells. *Journal of Unconventional Oil and Gas Resources*, 7:62-70.
https://doi.org/10.1016/j.juogr.2014.01.002

Nicoleau L, Schreiner E, Nonat A, 2014. Ion-specific effects influencing the dissolution of tricalcium silicate. *Cement and Concrete Research*, 59:118-138.
https://doi.org/10.1016/j.cemconres.2014.02.006

Ouyang XP, Guo YX, Qiu XQ, 2008. The feasibility of synthetic surfactant as an air entraining agent for the cement matrix. *Construction and Building Materials*, 22(8):1774-1779.
https://doi.org/10.1016/j.conbuildmat.2007.05.002

Palomo A, Macias A, Blanco MT, et al., 1992. Physical, chemical and mechanical characterization of geopolymers. Proceedings of the 9th International Congress on the Chemistry of Cement, p.505-511.

Park SM, Jang JG, Lee NK, et al., 2016. Physicochemical properties of binder gel in alkali-activated fly ash/slag exposed to high temperatures. *Cement and Concrete Research*, 89:72-79.
https://doi.org/10.1016/j.cemconres.2016.08.004

Partyka S, Zaini S, Lindheimer M, et al., 1984. The adsorption of non-ionic surfactants on a silica gel. *Colloids and Surfaces*, 12:255-270.
https://doi.org/10.1016/0166-6622(84)80104-3

Parveen S, Rana S, Fangueiro R, et al., 2015. Microstructure and mechanical properties of carbon nanotube reinforced cementitious composites developed using a novel dispersion technique. *Cement and Concrete Research*, 73: 215-227.
https://doi.org/10.1016/j.cemconres.2015.03.006

Pauling LC, 1949. A resonating-valence-bond theory of metals and intermetallic compounds. *Proceedings of the Royal Society A: Mathematical, Physical and Engineering Sciences*, 196(1046):343-362.
https://doi.org/10.1098/rspa.1949.0032

Provis JL, van Deventer JSJ, 2013. Alkali Activated Materials: State-of-the-art Report, RILEM TC 224-AAM. Springer, Dordrecht, the Netherlands.
https://doi.org/10.1007/978-94-007-7672-2

Rodríguez ED, Bernal SA, Provis JL, et al., 2013. Effect of nanosilica-based activators on the performance of an alkali-activated fly ash binder. *Cement and Concrete Composites*, 35(1):1-11.
https://doi.org/10.1016/j.cemconcomp.2012.08.025

Romero E, Simms PH, 2008. Microstructure investigation in unsaturated soils: a review with special attention to contribution of mercury intrusion porosimetry and environmental scanning electron microscopy. *Geotechnical and Geological Engineering*, 26(6):705-727.
https://doi.org/10.1007/s10706-008-9204-5

Rovnaník P, 2010. Effect of curing temperature on the development of hard structure of metakaolin-based geopolymer. *Construction and Building Materials*, 24(7):1176-1183.
https://doi.org/10.1016/j.conbuildmat.2009.12.023

Rowles M, O'connor B, 2003. Chemical optimisation of the compressive strength of aluminosilicate geopolymers synthesised by sodium silicate activation of metakaolinite. *Journal of Materials Chemistry*, 13(5):1161-1165.
https://doi.org/10.1039/b212629j

Saleh TA, Ali I, 2018. Synthesis of polyamide grafted carbon microspheres for removal of rhodamine B dye and heavy metals. *Journal of Environmental Chemical Engineering*, 6(4):5361-5368.
https://doi.org/10.1016/j.jece.2018.08.033

Saleh TA, Al-Saadi AA, Gupta VK, 2014. Carbonaceous adsorbent prepared from waste tires: experimental and computational evaluations of organic dye methyl orange. *Journal of Molecular Liquids*, 191:85-91. https://doi.org/10.1016/j.molliq.2013.11.028

Saleh TA, Tuzen M, Sarı A, 2018. Polyamide magnetic palygorskite for the simultaneous removal of Hg(II) and methyl mercury; with factorial design analysis. *Journal of Environmental Management*, 211:323-333. https://doi.org/10.1016/j.jenvman.2018.01.050

Samson G, Cyr M, 2018. Porous structure optimisation of flash-calcined metakaolin/fly ash geopolymer foam concrete. *European Journal of Environmental and Civil Engineering*, 22(12):1482-1498. https://doi.org/10.1080/19648189.2017.1304285

Sarda S, Nilsson M, Balcells M, et al., 2003. Influence of surfactant molecules as air-entraining agent for bone cement macroporosity. *Journal of Biomedical Materials Research Part A*, 65A(2):215-221. https://doi.org/10.1002/jbm.a.10458

SBQTS (State Bureau of Quality and Technical Supervision), 1999. Method of Testing Cements–Determination of Strength, GB/T 17671-1999. National Standards of the People's Republic of China (in Chinese).

Shi CJ, Krivenko PV, Roy D, 2006. Alkali-activated Cements and Concretes. Taylor & Francis, London, UK.

Slavik R, Bednarik V, Vondruska M, et al., 2008. Preparation of geopolymer from fluidized bed combustion bottom ash. *Journal of Materials Processing Technology*, 200(1-3):265-270. https://doi.org/10.1016/j.jmatprotec.2007.09.008

Szekely J, Neumann AW, Chuang YK, 1971. The rate of capillary penetration and the applicability of the washburn equation. *Journal of Colloid and Interface Science*, 35(2):273-278. https://doi.org/10.1016/0021-9797(71)90120-2

Tadros TF, 2005. Applied Surfactants: Principles and Applications. Wiley-VCH, Weinheim, Germany.

Tchakouté HK, Fotio D, Rüscher CH, et al., 2018. The effects of synthesized calcium phosphate compounds on the mechanical and microstructural properties of metakaolin-based geopolymer cements. *Construction and Building Materials*, 163:776-792. https://doi.org/10.1016/j.conbuildmat.2017.12.162

Turner LK, Collins FG, 2013. Carbon dioxide equivalent (CO_2-e) emissions: a comparison between geopolymer and OPC cement concrete. *Construction and Building Materials*, 43:125-130. https://doi.org/10.1016/j.conbuildmat.2013.01.023

Uchikawa H, Hanehara S, Shirasaka T, et al., 1992. Effect of admixture on hydration of cement, adsorptive behavior of admixture and fluidity and setting of fresh cement paste. *Cement and Concrete Research*, 22(6):1115-1129. https://doi.org/10.1016/0008-8846(92)90041-S

Wang BM, Zhang Y, 2014. Synthesis and properties of carbon nanofibers filled cement-based composites combined with new surfactant methylcellulose. *Materials Express*, 4(2):177-182. https://doi.org/10.1166/mex.2014.1157

Wang BM, Deng S, 2019. Effect and mechanism of graphene nanoplatelets on hydration reaction, mechanical properties and microstructure of cement composites. *Construction and Building Materials*, 228:116720. https://doi.org/10.1016/j.conbuildmat.2019.116720

Yan DM, Chen SK, Zeng Q, et al., 2016. Correlating the elastic properties of metakaolin-based geopolymer with its composition. *Materials & Design*, 95:306-318. https://doi.org/10.1016/j.matdes.2016.01.107

Yang K, Yi ZL, Jing QF, et al., 2014. Dispersion and aggregation of single-walled carbon nanotubes in aqueous solutions of anionic surfactants. *Journal of Zhejiang University-SCIENCE A (Applied Physics & Engineering)*, 15(8):624-633. https://doi.org/10.1631/jzus.A1400113

Yuan ZY, Zhou WZ, Su BL, et al., 2002. Mesoporous silicas of hierarchical structure by hydrothermal surfactant-templating under mild alkali conditions. *Studies in Surface Science and Catalysis*, 141:133-140. https://doi.org/10.1016/S0167-2991(02)80534-1

Zhang T, Shang S, Yin F, et al., 2001. Adsorptive behavior of surfactants on surface of Portland cement. *Cement and Concrete Research*, 31(7):1009-1015. https://doi.org/10.1016/S0008-8846(01)00511-7

Zhang Z, Wang H, 2015. Analysing the relation between pore structure and permeability of alkali-activated concrete binders. *In*: Pacheco-Torgal F, Labrincha JA, Leonelli C, et al. (Eds.), Handbook of Alkali–Activated Cements, Mortars and Concretes. Woodhead Publishing, Cambridge, UK, p.235-264. https://doi.org/10.1533/9781782422884.2.235

Zhao L, Guo XL, Liu YY, et al., 2018. Investigation of dispersion behavior of GO modified by different water reducing agents in cement pore solution. *Carbon*, 127:255-269. https://doi.org/10.1016/j.carbon.2017.11.016

Zhao WR, Shi HX, Wang DH, 2004. Modeling of mass transfer characteristics of bubble column reactor with surfactant present. *Journal of Zhejiang University-SCIENCE*, 5(6):714-720. http://doi.org/10.1631/jzus.2004.0714

Zuda L, Rovnaník P, Bayer P, et al., 2008. Effect of high temperatures on the properties of alkali activated aluminosilicate with electrical porcelain filler. *International Journal of Thermophysics*, 29(2):693-705. https://doi.org/10.1007/s10765-007-0311-y